High Performance Motion Control for Optical Satellite Tracking Systems

Thomas Riel*, Andras Galffy, Georg Janisch, Daniel Wertjanz, Andreas Sinn, Christian Schwaer, Georg Schitter

Automation and Control Institute (ACIN), TU Wien, Gußhausstraße 27-29, 1040, Vienna, Austria

Abstract

This paper investigates the motion control system of an optical tracking system used for precision satellite tracking and ranging applications. The system uses direct-drive permanent magnet synchronous motors (PMSMs) for high precision positioning. To overcome the performance limitations due to system dynamics and position dependent plant variations, a disturbance observer based control system is utilized. This paper contributes the detailed analysis, design and implementation of such an advanced control concept for the performance improvement of precision satellite tracking systems. Satellite tracking experiments are conducted to verify the performance of the proposed system. Utilizing the proposed control concept, the RMS servo error is reduced by a factor of 3.8 to well below the arcsecond range, achieving seeing limited tracking.

Keywords: Satellite Tracking, Precision Motion Control, Space Debris Observation, Satellite Laser Ranging, Optical Satellite Communication, Space Situation Awareness

1. Introduction

Precise motion control is required for a range of different applications. Especially optical satellite communication and space observation systems strive for a tracking precision that is in the sub-arcsecond range to enable seeing limited performance (Hemmati et al. (2011); Kaushal and Kaddoum (2017)). This level of performance should be maintained over the entire operational range and for velocities from standstill to the degrees per second (dps) range. Given the dynamic behavior of typical observation platforms with a large amount of low frequency dynamics, this is a challenging task for control system design.

*Corresponding author
Email address: riel@acin.tuwien.ac.at (Thomas Riel)

Pre-Print version of the article: Thomas Riel, Andras Galffy, Georg Janisch, Daniel Wertjanz, Andreas Sinn, Christian Schwaer, Georg Schitter, "High performance motion control for optical satellite tracking systems", *Advances in Space Research*, vol. 65, pp. 1333-1343, 2020. DOI: 10.1016/j.asr.2019.11.039

Similar systems, used for satellite tracking and ranging applications, are reported in literature to achieve root mean square (RMS) tracking errors between $0.3''$ to $2.4''$ (Park et al. (2012); Zhang et al. (2012); Riesing et al. (2017)).

The 40 cm accurate ranging system for geodetic observation - mobile (ARGO-M) satellite laser ranging (SLR) system is actuated by direct-drive permanent magnet synchronous motor (PMSM) and the position is measured using two optical encoders per axis (Park et al. (2012)). It achieves a peak tracking error for low earth orbit (LEO) satellites of $1.7''$ at the point of the maximum velocity, and less than $0.3''$ error over an exemplary trajectory.

The 60 cm SLR system at the Shanghai Observatory reports a servo-tracking performance with an error of less than $1''$ (Zhang et al. (2012)).

The Massachusetts Institute of Technology portable telescope for lasercom (MIT-PorTeL) is a low cost ground station intended for optical communication to nano satellites (Riesing et al. (2017)). It utilizes a commercial 28 cm Schmidt-Cassegrain system and achieves a tracking precision for LEO satellites of $65''$ RMS. The system then utilizes an active tracking approch with additional tip-tilt mirror to achieve a RMS tracking error of $2.4''$. In contrast to the previous systems, the goal of this system is to reduce the cost for optical ground stations (OGSs) by a factor of 100, from several million USD to approx. 50kUSD.

In the control of the reported systems, cascaded proportional-integral (PI) controllers are applied (Park et al. (2012)). They have the advantage of being intuitive and simple to implement. However, future applications require even higher performance while demanding more robust, cost efficient and mobile solutions.

To achieve these goals, advanced control concepts have been investigated (Erm et al. (2004); Gawronski (2007); Riel et al. (2017a, 2018)). The use of H_∞ controller design has been proposed for the control of large structures, such as radio dishes (Gawronski (2007)). The advantage of H_∞ control has also been investigated in a simulation study for the very large telescope (VLT) (Erm et al. (2004)). The potential benefits of applying advanced control, such as disturbance observer (DOB) based control, have been investigated and demonstrated for small systems in a laboratory environment (Riel et al. (2017a)).

DOB based control systems (Ohnishi et al. (1996); Chen et al. (2016)) have been implemented successfully in a variety of precision positioning applications (Jamaludin et al. (2009); Yang et al. (2017)). The application of DOB based control for linear PMSM drive with additional friction model yields improved tracking performance (Jamaludin et al. (2009)). The utilization of DOB based control of a x-y motion stage in presence of significant plant dynamics has also been investigated and shows performance improvements (Yang et al. (2017)). Also the stability of DOB based control systems in presence of plant variations and velocity dependent behavior have been analyzed and proves the robust performance (Riel et al. (2018)). However, the application of such a system in a real satellite tracking applications has not yet been demonstrated.

Pre-Print version of the article: Thomas Riel, Andras Galffy, Georg Janisch, Daniel Wertjanz, Andreas Sinn, Christian Schwaer, Georg Schitter, "High performance motion control for optical satellite tracking systems", *Advances in Space Research*, vol. 65, pp. 1333-1343, 2020. DOI: 10.1016/j.asr.2019.11.039

This paper presents the design, implementation and verification of a DOB based control system for an optical tracking system used for precision satellite tracking and ranging applications. The used platform can be positioned with direct-drive PMSMs and has been optimized for high precision motions (Riel et al. (2017b)). To the best of the author's knowledge, this is the first time the design, implementation and verification of such a control system for optical tracking is reported. Feedback control in combination with a loop shaping filter and DOB is investigated. The pose dependent changes in the system dynamics are investigated. A loop shaping filter is implemented to reach robust performance and stability of the system. Experimental verification, using LEO and medium earth orbit (MEO) satellites, confirm the improved tracking performance of the proposed control system.

The remaining paper is organized as follows. Section 2 provides a brief description of the investigated system. A physical model of the system is presented in Section 3. The system identification and parameter estimation is described in Section 4. The identified model is then used in Section 5 to design a controller and analyze its robust stability. Satellite tracking experiments are shown to evaluate and demonstrate the proposed control system in Section 6. Finally, the conclusion is presented in Section 7.

2. System description

The investigated system, shown in Figure 1, is intended as a cost effective prototype of a semi-mobile ground station developed together with the industrial partner. The system is intended for optical satellite communication, SLR, space debris observation, as well as scientific investigations. As such, the platform should be able to move with a velocity of up to one dps, while retaining a servo error in the sub-arcsecond range. These specifications should allow the station to track MEO, as well as LEO satellites with seeing limited precision (Kirchner et al. (2006)). The intended cost of the system is close to the target of the MIT-PorTeL (Riesing et al. (2017)) and therefor at least one order of magnitude below other high performance tracking systems.

The system is actuated by two direct-drive PMSMs with eleven pole pairs and a rated torque of 6.3 N m and 14.1 N m, respectively. An overview of the PMSM parameters is presented in Table 1. The position of the system is determined by optical encoders with a noise floor below 160 nrad RMS. The optical system has 30 cm diameter with a flat tertiary mirror and a 5.5 Megapixel sCMOS camera (Zyla 5.5, Andor Technology Ltd, Belfast, Northern Ireland). The tertiary mirror and camera are mounted on an optical breadboard, which is fixed to the tube using clamps (see Figure 1). The two mount axes are arranged to align with the altitude (alt) and azimuth (az) axes. The system is attached to a solid support or tripod by four screws and can easily be transported using a medium sized car.

Pre-Print version of the article: Thomas Riel, Andras Galffy, Georg Janisch, Daniel Wertjanz, Andreas Sinn, Christian Schwaer, Georg Schitter, "High performance motion control for optical satellite tracking systems", *Advances in Space Research*, vol. 65, pp. 1333-1343, 2020. DOI: 10.1016/j.asr.2019.11.039

Figure 1: Investigated platform for satellite tracking, mounted on a rooftop in Upper Austria near Linz. Also visible is the optical breadboard with tertiary mirror and camera.

Table 1: Motor parameter of the two axis.

	alt-axis	az-axis
Rated current I_{nom}	3.4A	5.8A
Number of pole pairs Z_{p}	11	11
Resistance R	$1.31\,\Omega$	$0.98\,\Omega$
Inductance L_{q}	3.3 mH	5.4 mH
Torque constant k_{m}	1.84 N m/A	2.43 N m/A

The system shows significant dynamics in the low frequency range, which limits the achievable precision using PI control to several arcseconds (Riel et al. (2016a)). This is not sufficient for the intended applications which strive for seeing limited precision. In order to develop and implement advanced control concepts, a model of the system dynamics is obtained in the next section.

3. System modeling

For the purpose of controller design, each axis is modeled by a simple electromechanical model (Riel et al. (2016b, 2017b)). The mechanical part of the

Pre-Print version of the article: Thomas Riel, Andras Galffy, Georg Janisch, Daniel Wertjanz, Andreas Sinn, Christian Schwaer, Georg Schitter, "High performance motion control for optical satellite tracking systems", *Advances in Space Research*, vol. 65, pp. 1333-1343, 2020. DOI: 10.1016/j.asr.2019.11.039

model is described as a lumped mass system

$$\frac{\mathrm{d}\varphi}{\mathrm{d}t} = \omega \tag{1a}$$

$$\frac{\mathrm{d}\omega}{\mathrm{d}t} = \frac{1}{J}\left(T_{\mathrm{e}} - T_{\mathrm{l}}\right), \tag{1b}$$

where φ is the angular position, ω the angular velocity, J the moment of inertia, T_{e} the electrical torque, and T_{l} describes the total disturbance torque. As such, T_{l} includes friction effects as well as gravitational loads and external disturbances such as wind shake or vibrations.

The electrical part is described using a simple PMSM model given by

$$\frac{\mathrm{d}i_{\mathrm{d}}}{\mathrm{d}t} = \frac{1}{L_{\mathrm{d}}}\left(u_{\mathrm{d}} - R\, i_{\mathrm{d}} + \omega_e\, L_{\mathrm{q}}\, i_{\mathrm{q}}\right) \tag{2a}$$

$$\frac{\mathrm{d}i_{\mathrm{q}}}{\mathrm{d}t} = \frac{1}{L_{\mathrm{q}}}\left(u_{\mathrm{q}} - R\, i_{\mathrm{q}} + \omega_e\, L_{\mathrm{d}}\, i_{\mathrm{d}} - \omega_e\, \Psi_{\mathrm{M}}\right), \tag{2b}$$

where $L_{\mathrm{d}}, L_{\mathrm{q}}$ are the d, q reference frame inductances, $u_{\mathrm{d}}, u_{\mathrm{q}}$ the d, q reference frame stator voltages, R the stator resistance, $i_{\mathrm{d}}, i_{\mathrm{q}}$ the d, q reference frame stator currents, Ψ_{M} the mutual magnetic flux due to the rotor magnets and $\omega_e = Z_{\mathrm{p}}\,\omega$ the electrical velocity with Z_{p} as the number of pole pairs.

The connection of the electrical and mechanical part is formed by the generated electrical torque

$$T_{\mathrm{e}} = \frac{3}{2} Z_{\mathrm{p}}\left(\Psi_{\mathrm{M}}\, i_{\mathrm{q}} + \left(L_{\mathrm{d}} - L_{\mathrm{q}}\right) i_{\mathrm{d}}\, i_{\mathrm{q}}\right). \tag{3}$$

A cascaded current controller is used to control the electrical subsystem of the PMSM with a bandwidth of close to 1 kHz. This allows the substitution of $i_q = i_q^{des}$ and $i_d = i_d^{des} = 0$. As a consequence of this substitution, the electromechanical model, (1a)-(3), is reduced to

$$\frac{d\varphi}{dt} = \omega \tag{4a}$$

$$\frac{d\omega}{dt} = \frac{1}{J}\left(k_M\, i_q^{des} - T_l\right), \tag{4b}$$

with the motor constant $k_M = \frac{3}{2} Z_{\mathrm{p}}\, \Psi_{\mathrm{M}}$. The model (4) represents the rigid body behavior of the axis without system dynamics.

4. Parameter estimation and system identification

The model (4), as presented in Section 3, contains a number of parameters that need to be determined. In addition, the flexible system dynamics need to be identified.

Pre-Print version of the article: Thomas Riel, Andras Galffy, Georg Janisch, Daniel Wertjanz, Andreas Sinn, Christian Schwaer, Georg Schitter, "High performance motion control for optical satellite tracking systems", *Advances in Space Research*, vol. 65, pp. 1333-1343, 2020. DOI: 10.1016/j.asr.2019.11.039

4.1. Parameter estimation

The least squares method (Ljung (1987)) is used to estimate the parameters of the model (4). A 1 Hz rectangular signal with 0.5 A amplitude is applied as the quadrature current reference. The result of this excitation is recorded and used to fit the simple model

$$\frac{d\omega}{dt} = \frac{k_m}{J}\, i_q^{des} - \frac{\beta}{J}\omega - \frac{T_c}{J}\,\mathrm{sign}(\omega) - \frac{T_u(\varphi)}{J}, \tag{5}$$

where β is the viscous friction parameter, T_c is the coulomb friction moment and T_u is the unbalance moment. T_u is given by $m_u\, g\, a_u\, \sin(\varphi - \varphi_0)$, with the mass and center distance of the lumped mass imbalance of the axis, m_u and a_u, and the balanced position φ_0.

Using the model (5), the parameters for estimation are $c_M = \frac{k_m}{J}$, $c_v = \frac{\beta}{J}$, $c_c = \frac{T_c}{J}$, and $c_u = \frac{m_u\, g\, a_u}{J}$. The parameter φ_0 is determined prior to the identification by measurement of the idle position before the axis is activated. The position φ is measured with the optical encoder and the kinematic states $\dfrac{d\varphi}{dt}$ and $\dfrac{d\omega}{dt}$ are derived thereof by numeric differentiation. The actual quadrature current i_q^{des} is extracted from the internal current control.

Once identified, the parameter $c_M = \frac{k_m}{J}$ is then used for the model (4).

4.2. System identification

Apart from the parameter estimation, also the system dynamics, which are not covered by the rigid body model (4), need to be identified to investigate the stability of the control system. Sweeped sine frequency response data are used to identify the system dynamics in closed loop configuration (Pintelon and Schoukens (2012)). The quadrature current reference is used as input signal and the position of the optical encoder is used as output. The axis under investigation is subjected to a constant velocity motion of $0.001\,\frac{\mathrm{rad}}{\mathrm{s}}$ during the measurement. This slow motion prevents the measurement to be influenced by non-linear friction phenomena but introduces additional noise, especially at lower frequencies.

The measurement is repeated at various positions, spanning the entire working range, to analyze the variation of the system behavior. The resulting frequency response data are shown in Figure 2 for the alt-axis and in Figure 3 for the az-axis. In both axes, a dominant anti-resonance/resonance pair is observed at 30 Hz/300 Hz for the alt-axis and 12 Hz/40 Hz for the az-axis. This indicates a decoupling of the tube from the mount above theses resonance frequencies. Targeting a control bandwidth above this frequencies is therefor ineffective.

Figure 2 indicates a significant variation in the quality factor of a resonance at 240 Hz. In addition, several resonances between 40 Hz and 150 Hz appear to be linked to the position of the axes. Resonances at 440 Hz and beyond appear to be unaffected by the change in position. From a previous finite element analysis, it is known that the several modes of the U-shaped mount fork appear in the 10 Hz to

Pre-Print version of the article: Thomas Riel, Andras Galffy, Georg Janisch, Daniel Wertjanz, Andreas Sinn, Christian Schwaer, Georg Schitter, "High performance motion control for optical satellite tracking systems", *Advances in Space Research*, vol. 65, pp. 1333-1343, 2020. DOI: 10.1016/j.asr.2019.11.039

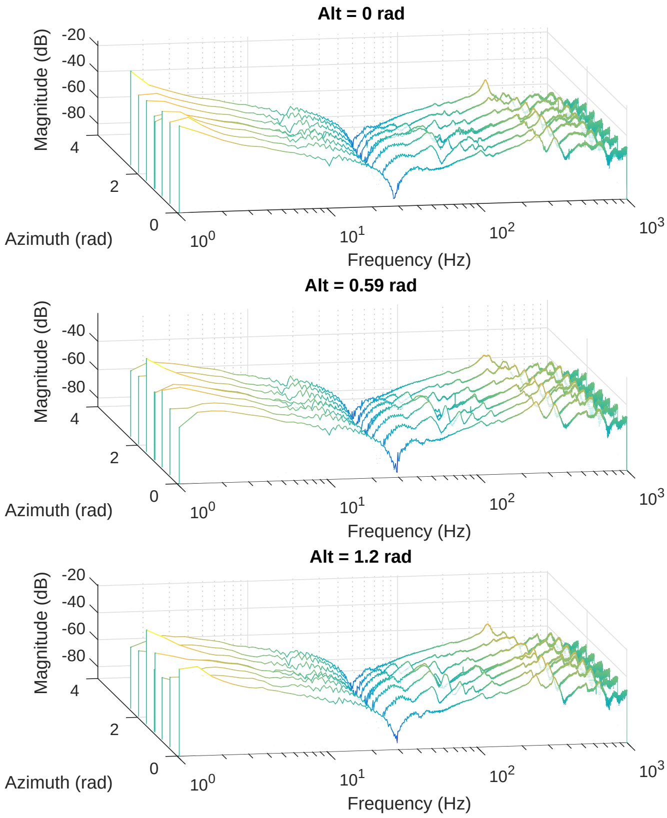

Figure 2: Magnitude of the frequency response of the alt-axis (i_q to ω) for various alt and az positions.

200 Hz range. These modes are also dependent on the pose of the mount. Several modes of individual parts, e.g. the counterweight shaft, appear at frequencies beyond 300 Hz. These modes are independent of the tube position.

The measurement of the az-axis, shown in Figure 3, indicates a significant variation of the resonances between 8 Hz to 15 Hz with the position of the axis. Another resonance appears to shift between 240 Hz and 290 Hz in response to a variation in the az position. The resonances at 40 Hz and a number of resonances beyond 300 Hz show no significant variation by the change in position.

Using these frequency response data, the control system can be designed and its stability analyzed.

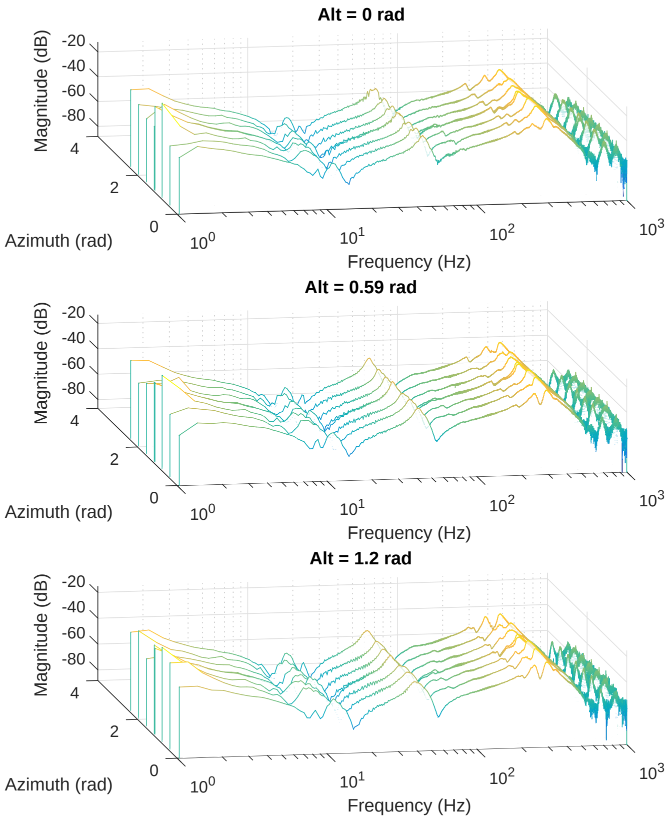

Figure 3: Magnitude of the frequency response of the az-axis (i_q to ω) for various alt and az positions.

5. Control system design and stability analysis

The use of DOB based control has proven effective for mechatronic motion systems (Ohnishi et al. (1996); Chen et al. (2016)). It employs an observer to estimate the effect of an unmeasurable but observable, external disturbance. The estimate of the disturbance is then used to adjust the control action, thereby compensating the disturbance. As a consequence, not only external disturbances are rejected, but also unmodeled dynamics and parameter variations can be compensated for.

5.1. Disturbance observer

The model (4), presented in Section 3, is used to design an extended state observer (Riel et al. (2017a))

$$\frac{d\hat{\varphi}}{dt} = \hat{\omega} + k_{1,o}\, e_\varphi \tag{6a}$$

$$\frac{d\hat{\omega}}{dt} = \hat{c}_M\, i_q^{des} + \hat{\alpha}_l + k_{2,o}\, e_\varphi \tag{6b}$$

$$\frac{d\hat{\alpha}_l}{dt} = k_{3,o}\, \hat{e}_{\varphi,I} + k_{4,o}\, e_\varphi \tag{6c}$$

$$\frac{d\hat{e}_{\varphi,I}}{dt} = e_\varphi, \tag{6d}$$

where $\hat{\varphi}$, $\hat{\omega}$ are the estimated kinematic states, α_l is the acceleration due to disturbances, $e_\varphi = \varphi - \hat{\varphi}$ is the position estimation error, $\hat{c}_M = \frac{k_M}{J}$ is the estimated system parameter, and $k_{1,o}$ to $k_{4,o}$ are the observer gains. The variables i_q^{des} and φ are the two measured inputs to the observer. In addition to the kinematic states and the acceleration due to disturbances $\alpha_l = \frac{T_l}{J}$, the additional state $e_{\varphi,I}$ is introduced. This provides additional integrating behavior for the position estimation error e_φ.

Figure 4 depicts a block diagram of the proposed motion control system with a trajectory generator G_T, state feedback controller G_C and $G_P^{'}$ as the augmented plant, which is formed by the DOB loop. Within the DOB loop, the state of the plant G_P is estimated by the disturbance observer G_O. A loop shaping filter Q is utilized to ensure robust stability of the system by suppressing unmodeled dynamics. An additional delay line compensates the time delay of G_P. To cancel the disturbance d acting on the plant, the estimated disturbance $\hat{\alpha}_l$ is applied as additional input to the plant, i.e.

$$i_q^{des} = \frac{u - \hat{\alpha}_l}{\hat{c}_M}, \tag{7}$$

where u is the control action of the superordinate motion controller.

The separation principle (Åström and Wittenmark (1997)) allows the separate configuration of observer and controller. The bandwidth of the observer is

Pre-Print version of the article: Thomas Riel, Andras Galffy, Georg Janisch, Daniel Wertjanz, Andreas Sinn, Christian Schwaer, Georg Schitter, "High performance motion control for optical satellite tracking systems", *Advances in Space Research*, vol. 65, pp. 1333-1343, 2020. DOI: 10.1016/j.asr.2019.11.039

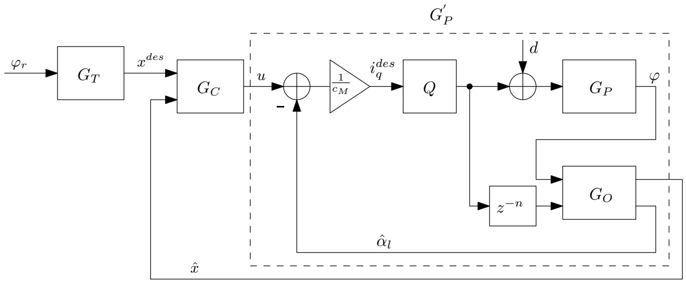

Figure 4: Block diagram of the motion control system with the trajectory generator G_T, state feedback controller G_C and the DOB loop G_P', where the disturbance observer G_O is used to estimate the states of the plant G_P, while a loop shaping filter Q is utilized to ensure robust stability.

set by pole-placement. The used bandwidth is set a factor of ten higher than the targeted closed loop bandwidth of the motion controller, which results in a bandwidth of 100 Hz.

5.2. Robust stability analysis and loop shaping

Based on the frequency response data shown in Figure 2 and Figure 3 two robust controllers are designed: A PI controller and a DOB based control system. The PI controller is later used as a benchmark for the experimental comparison of the DOB based control system.

5.2.1. Proportional-integral control

The PI control bandwidth is limited by the gain margin of several resonances in each axis. To suppress these high frequency dynamics, additional second order lowpass filter are used at ten times the desired control bandwidth. Using this model free approach, the control bandwidth is limited to 4 Hz and 2.5 Hz for the alt and az-axis, respectively. To overcome these limitations a DOB based control system with loop shaping filter is designed in the following subsection.

5.2.2. Disturbance observer based control

When considering an observer with stable poles at frequencies that are sufficiently higher than the dynamics of the feedback, then the separation principle applies. This leads to closed loop dynamics of the DOB loop which are determined by the dynamics of the feedback control system. For the frequency range that is within the bandwidth of the observer, the relationship $T = Q$ applies, where T is the complementary sensitivity function of the DOB loop (Kempf and Kobayashi (1999)).

As a consequence, frequency response data can be used to investigate robust stability. The shaping filter Q is used to shape the feedback dynamics accordingly.

Pre-Print version of the article: Thomas Riel, Andras Galffy, Georg Janisch, Daniel Wertjanz, Andreas Sinn, Christian Schwaer, Georg Schitter, "High performance motion control for optical satellite tracking systems", *Advances in Space Research*, vol. 65, pp. 1333-1343, 2020. DOI: 10.1016/j.asr.2019.11.039

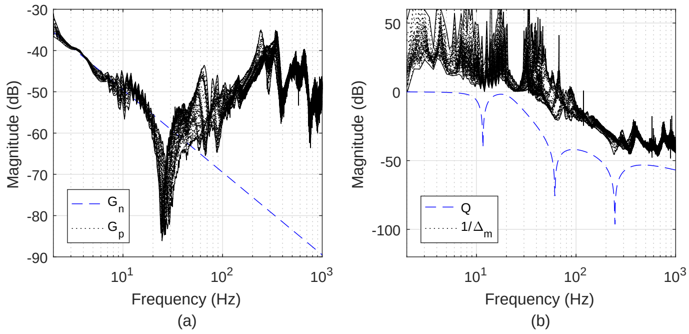

Figure 5: (a) Magnitude of the nominal plant model G_n as presented in (4) (blue, dashed), together with the identified frequency response data of the alt-axis (i_q to ω, black, dotted). (b) Magnitude of the loop shaping filter Q for the alt-axis (blue, dashed) together with the reciprocal of the multiplicative plant perturbation Δ_m (black, dotted).

The shaping filter is implemented using four digital biquad filter sections, which allows a maximal filter order of eight. Three filter types, elliptic lowpass, notch and butterworth lowpass, can be selected, parametrized and implemented using a user interface. Matlab is used to calculate the filter coefficients of the biquad filter.

To guarantee robust stability, the DOB loop has to fulfill the condition (Doyle et al. (2009))

$$\|Q\|_\infty < \frac{1}{\|\Delta_m\|_\infty}, \tag{8}$$

where Δ_m is the multiplicative plant perturbation and Q is the shaping filter. The multiplicative plant perturbation is defined by $G_p = G_n(1+\Delta_m)$, where G_p and G_n are the perturbed and nominal plant, respectively. As such, $\frac{1}{\Delta_m}$ is given by

$$\frac{1}{\Delta_m} = \frac{G_n}{G_p - G_n}. \tag{9}$$

Condition (8) is imposed by forming the shaping filter Q accordingly, i.e. reducing the gain of Q at frequencies with large uncertainty. Figure 5 and Figure 6 illustrate the realization of the shaping filter of the alt and az-axis, respectively. This manual method of realizing the shaping filter Q might be counter intuitive, as mathematical frameworks for finding an optimal Q exist in control literature (Zhou et al. (1996)). However, as the system configuration is regularly changed, e.g. changing the detector, it is necessary to also change the Q filter accordingly. The tracking system operator should be able to carry out this task, therefor a intuitive and simple filter implementation was chosen, such that the operator can easily adjust the filter in the field.

The shaping filter for the alt-axis is of seventh order. It is comprised of an

Pre-Print version of the article: Thomas Riel, Andras Galffy, Georg Janisch, Daniel Wertjanz, Andreas Sinn, Christian Schwaer, Georg Schitter, "High performance motion control for optical satellite tracking systems", *Advances in Space Research*, vol. 65, pp. 1333-1343, 2020. DOI: 10.1016/j.asr.2019.11.039

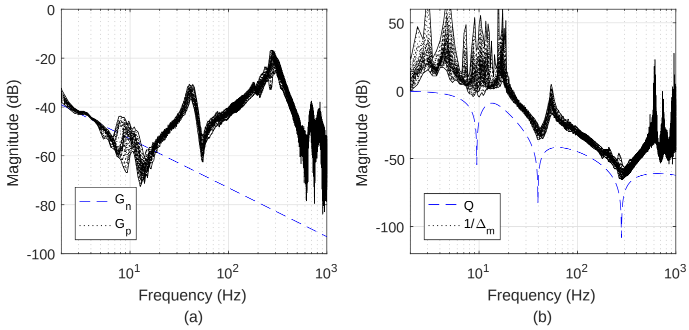

Figure 6: (a) Magnitude of the nominal plant model G_n as presented in (4) (blue, dashed), together with the identified frequency response data of the az-axis (i_q to ω, black, dotted). (b) Magnitude of the loop shaping filter Q for the az-axis (blue, dashed) together with the reciprocal of the multiplicative plant perturbation Δ_m (black, dotted).

elliptic lowpass of third order and two additional second order notch filter. The elliptic filter has a cutoff frequency of 17 Hz and a pair of zero at 65 Hz. The first notch filter has a center frequency of 12 Hz and a quality factor ($= f_c/f_{-3dB}$) of two. The second notch filter has a center frequency of 240 Hz and a quality factor of 1.7.

The shaping filter for the az-axis is of seventh order. It is comprised of an elliptic lowpass of third order and two additional second order notch filters. The elliptic filter has a cutoff frequency of 8 Hz and a pair of zero at 37 Hz. The first notch filter has a center frequency of 9 Hz and a quality factor of two. The second notch filter has a center frequency of 280 Hz and a quality factor of 1.4.

5.3. Motion controller design

A state feedback motion controller is used in conjunction with the DOB. A schematic representation of the motion control system is shown in Figure 4. The estimated kinematic state $\hat{x} = [\hat{\varphi}, \hat{\omega}]^T$, that is provided by the disturbance observer, is used in the feedback loop. The utilized controller is given by

$$\begin{aligned} u = {} & k_{1,r}\,(\varphi^{des} - \hat{\varphi}) + k_{2,r}\,(\omega^{des} - \hat{\omega}) + \alpha^{des} \\ & + k_{3,r}\,\epsilon_{\varphi,I,r}, \end{aligned} \tag{10}$$

where α^{des}, ω^{des} and φ^{des} are the desired acceleration, velocity and position, $k_{1,r}$ to $k_{3,r}$ are the controller gains, and $\epsilon_{\varphi,I,r}$ is the integral of the position error $\varphi^{des} - \hat{\varphi}$. With (10) and (7), the closed loop error dynamics of the feedback system of (4) can be written in matrix representation as

$$\frac{d\vec{\epsilon}}{dt} = \frac{d}{dt}\begin{bmatrix}\epsilon_{\varphi,I,r}\\ \epsilon_{\varphi}\\ \epsilon_{\omega}\end{bmatrix} = \begin{bmatrix}0 & 1 & 0\\ 0 & 0 & 1\\ -k_{I,r} & -k_{2,r} & -k_{1,r}\end{bmatrix}\begin{bmatrix}\epsilon_{\varphi,I,r}\\ \epsilon_{\varphi}\\ \epsilon_{\omega}\end{bmatrix}, \tag{11}$$

Pre-Print version of the article: Thomas Riel, Andras Galffy, Georg Janisch, Daniel Wertjanz, Andreas Sinn, Christian Schwaer, Georg Schitter, "High performance motion control for optical satellite tracking systems", *Advances in Space Research*, vol. 65, pp. 1333-1343, 2020. DOI: 10.1016/j.asr.2019.11.039

where ϵ_φ and ϵ_ω are the state errors $\varphi^{des} - \hat{\varphi}$ and $\omega^{des} - \hat{\omega}$, respectively.

The error $\vec{\epsilon}$ decays to $\vec{0}$ according to the characteristic polynomial $p_r(s) = s^3 + k_{1,r}\, s^2 + k_{2,r}\, s + k_{I,r}$.

The motion control bandwidth is defined by pole-placement, such that it follows a butterworth lowpass characteristic with the same bandwidth as the shaping filter. This results in a bandwidth of 9 Hz for the alt-axis and 5 Hz for the az-axis.

5.4. Trajectory generator design

The position reference φ_r is provided in the form of N^{th} order polynomials $\varphi_r(t) = \sum_{i=0}^{N} c_i t^i$, that are piecewise fitted to the predicted satellite trajectory in a continuous fashion. The trajectory generator G_T is used to calculate the desired values of α, ω and φ by analytic differentiation in the form

$$\alpha^{des}(t) = \sum_{i=2}^{N} i\,(i-1)\, c_i t^{i-2}, \tag{12a}$$

$$\omega^{des}(t) = \sum_{i=1}^{N} i\, c_i\, t^{i-1}, \tag{12b}$$

$$\varphi^{des}(t) = \sum_{i=0}^{N} c_i\, t^i. \tag{12c}$$

The position reference φ_r is fitted in sub-second intervals with 8^{th} order polynomials using the least squares method. The fitting residuals are in the nano-degree range. Using this configuration, the real-time requirements of the communication interface are relaxed and the full 20 kHz sampling rate of the motion controller can be utilized.

6. Experimental results

The proposed control system is evaluated using the setup described in Section 2. Various rocket bodies and satellites are used as test targets for blind tracking. The orbit of the objects is determined using two-line element sets (TLEs), which are sourced from *celestrak.com* (Kelso (2018)), or consolidated prediction format (CPF) data of the international laser ranging service (ILRS) (Pearlman et al. (2002)) sourced from *cddis.nasa.gov* (Noll (2018)). Following the orbit prediction, the trajectory is performed in an open-loop fashion without any visual feedback, i.e. blind tracking. A list of the used objects and the data reference used for predicting their orbit is shown in Table 2.

A GPS timing module is used as absolute time reference. The internal quartz oscillator is synchronized against the pulse-per-second (PPS) signal of the GPS timing module to guarantee a precise absolute time reference at each sampling step.

Pre-Print version of the article: Thomas Riel, Andras Galffy, Georg Janisch, Daniel Wertjanz, Andreas Sinn, Christian Schwaer, Georg Schitter, "High performance motion control for optical satellite tracking systems", *Advances in Space Research*, vol. 65, pp. 1333-1343, 2020. DOI: 10.1016/j.asr.2019.11.039

Table 2: Used objects for the tracking experiments.

Name	NORAD ID	Perigee	Apogee	Orbit Source
BREEZ-M DEB	36501	331 km	13 138 km	TLE
ISS	25544	409 km	415 km	TLE
CRYOSAT-2	36508	719 km	732 km	CPF
ENVISAT	27386	772 km	773 km	CPF
ATLAS 2AS CENTAUR R/B	26906	805 km	1398 km	TLE
H-2 R/B	24279	865 km	1314 km	TLE
THORAD AGENA D R/B	05679	937 km	953 km	TLE
USA 194 DEB	31708	941 km	1287 km	TLE
COSMOS-2344	24827	1278 km	2979 km	TLE
JASON-2	33105	1312 km	1324 km	CPF
JASON-3	41240	1339 km	1350 km	CPF
AJISAI	16908	1486 km	1504 km	CPF
LAGEOS-2	22195	5622 km	5959 km	CPF
ETALON-1	19751	19 077 km	19 189 km	CPF
GLONASS-102	29670	19 082 km	19 192 km	CPF
GLONASS-103	29671	19 092 km	19 182 km	CPF
GLONASS-126	37829	19 119 km	19 155 km	CPF
BEIDOU-3M3	43208	21 516 km	21 554 km	CPF
GALILEO-205	40889	23 221 km	23 238 km	CPF

Tracking experiments are performed for visible tracks only, i.e. when the satellite is illuminated by the sun in such a way that it is visible from the ground station. This allows additional posterior visual validation of the tracking results. Nevertheless, to evaluate the proposed control system, the servo error is used as indicator.

The tracking experiments have durations between 15 and 90 seconds and are performed at various altitudes, ranging from 25° to 81°. In total, 43 experiments are carried out over a duration of 16 days in September of 2018. To evaluate the proposed control system, several tracking experiments are conducted using the designed PI controller.

In Figure 7 and Figure 8, two exemplary tracklets are shown. Figure 7 shows a 26 second duration (excluding initial mount acceleration sequence) tracklet of the satellite JASON-2 (NORAD ID: 33105), recorded on the 20$^{\text{th}}$ of September 2018, 23:43:18 UTC. The trajectory has a maximal angular velocity of 0.4 dps and starts at an altitude of 51°. Figure 8 shows a 25 second duration tracklet of a debris segment of the rocket body Breeze-M (NORAD ID: 36501). The tracklet was recorded on the 18$^{\text{th}}$ of September 2018, 23:43:18 UTC. It has a

Pre-Print version of the article: Thomas Riel, Andras Galffy, Georg Janisch, Daniel Wertjanz, Andreas Sinn, Christian Schwaer, Georg Schitter, "High performance motion control for optical satellite tracking systems", *Advances in Space Research*, vol. 65, pp. 1333-1343, 2020. DOI: 10.1016/j.asr.2019.11.039

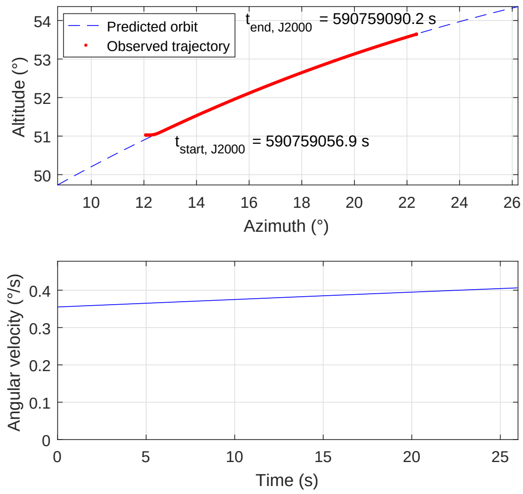

Figure 7: Tracklet with 26 seconds duration of the satellite JASON-2 (NORAD ID: 33105), recorded on the 20th of September 2018, 23:43:18 UTC, with a mean angular velocity of 0.38 dps. Also visible is the acceleration sequence at the start of the trajectory.

maximal angular velocity of 1 dps and starts at an altitude of 73°. In the first third of the tracklet, two obstructions are visible, where clouds blocked the visual observation. Both Figure 7 and Figure 8 also include the initial acceleration phase of the tracking system, visible at the start of the tracklet.

Figure 9 depicts a stacked image of twenty individual exposures of the satellite JASON-3 (NORAD ID: 41240), as it was observed on 27th of September 2018 at 00:09:36 UTC. The red square with 75″ size marks the satellite, while passing stars are visible as dashed lines.

To evaluate the performance of the proposed control system, a comparison to the PI control is shown in Figure 10.

Figure 10 indicates that on average, the servo error is reduced by a factor of 3.8 using the proposed control system when compared to the conventional PI control. For an exemplary tracking velocity of 0.8 dps, the RMS servo error is reduced from 3″ to below 0.75″. For velocities of up to 0.2 dps the error is below 0.5″. For velocities of up to 1 dps the error remains below 1″. This indicates that the achievable tracking performance is well below the average seeing conditions due to atmospheric turbulence, which reach several arcseconds (Kirchner et al. (2006)). Using the visual observations of the satellite tracklets to calculate the observed optical tracking error, it is found that this error ranges from 2″ to 5″ RMS. These values are close to the range previously reported by an Austrian SLR station (Kirchner et al. (2006)). This verifies the proposed control concept and

Pre-Print version of the article: Thomas Riel, Andras Galffy, Georg Janisch, Daniel Wertjanz, Andreas Sinn, Christian Schwaer, Georg Schitter, "High performance motion control for optical satellite tracking systems", *Advances in Space Research*, vol. 65, pp. 1333-1343, 2020. DOI: 10.1016/j.asr.2019.11.039

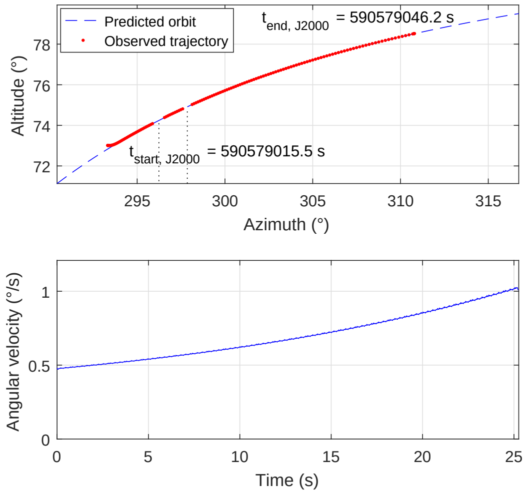

Figure 8: Tracklet with 25 seconds duration of debris of the rocket body Breeze-M (NORAD ID: 36501), recorded on the 18^{th} of September 2018, 21:43:35 UTC, with a mean angular velocity of 0.71 dps. Also visible is the acceleration sequence at the start of the trajectory and two obstructions due to cloud cover in the first third of the tracklet (at an az angle of 296° and 298°).

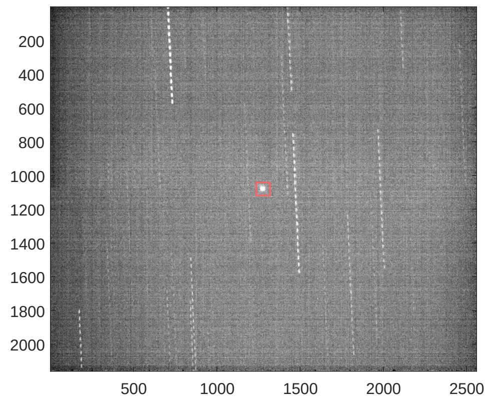

Figure 9: Stack of twenty images taken of the satellite JASON-3 (NORAD ID: 41240) on 27^{th} of September 2018 at 00:09:36 UTC. The satellite is marked with a red square of 75″ size. Passing stars can be seen as dashed lines in the stacked image.

Pre-Print version of the article: Thomas Riel, Andras Galffy, Georg Janisch, Daniel Wertjanz, Andreas Sinn, Christian Schwaer, Georg Schitter, "High performance motion control for optical satellite tracking systems", *Advances in Space Research*, vol. 65, pp. 1333-1343, 2020. DOI: 10.1016/j.asr.2019.11.039

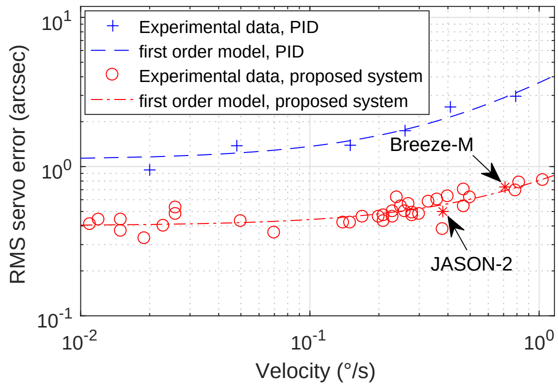

Figure 10: RMS servo error using standard PI control (blue, dashed) in comparison to the proposed control system (red, dash-dotted). Shown are the RMS servo errors of the performed tracklets as a function of the mean tracklet velocity. The two tracklets shown in Figure 9 and Figure 8 are marked by arrows.

fulfills the set requirements of retaining a servo precision in the sub-arcsecond range for tracking satellites at velocities from standstill to one dps.

7. Conclusion

An advanced control concept for high performance control of an optical satellite tracking system is proposed. The stability of the system in response to position dependent plant uncertainties is analyzed. A robust loop shaping approach together with a disturbance observer is used to guarantee robust stability over the entire operational range. Experimental verification is carried out using blind tracking of various satellites and rocket bodies. Compared to conventional PI control, by utilizing the proposed control concept, the average RMS servo error is reduced by a factor of 3.8, to below 0.5″ for velocities of up to 0.2 dps and below 1″ for velocities of up to 1 dps. This allows the system to operate with a tracking precision that is mainly limited by the atmospheric seeing conditions. Comparing the investigated, cost effective system to high performance systems presented in literature, very similar tracking performance is achieved.

Building on the obtained results, future work will focus on the investigation of the accuracy of the tracking system. Utilizing the proposed system, this future work shall enable highly accurate and precise blind tracking of satellites.

Acknowlegements

This work was funded by the Austrian research funding association (FFG) under the scope of the Bridge program (contract number 850722).

Pre-Print version of the article: Thomas Riel, Andras Galffy, Georg Janisch, Daniel Wertjanz, Andreas Sinn, Christian Schwaer, Georg Schitter, "High performance motion control for optical satellite tracking systems", *Advances in Space Research*, vol. 65, pp. 1333-1343, 2020. DOI: 10.1016/j.asr.2019.11.039

References

Hamid Hemmati, Abhijit Biswas, and Ivan B. Djordjevic. Deep-space optical communications: Future perspectives and applications. *Proceedings of the IEEE*, 99(11):2020–2039, 2011.

H. Kaushal and G. Kaddoum. Optical communication in space: Challenges and mitigation techniques. *IEEE Communications Surveys Tutorials*, 19(1):57–96, 2017.

Cheol Hoon Park, Young Su Son, Byung In Kim, Sang Young Ham, Sung Whee Lee, and Hyung Chul Lim. Design of tracking mount and controller for mobile satellite laser ranging system. *Advances in Space Research*, 49(1):177–184, 2012.

Zhong-Ping Zhang, Fu-Min Yang, Hai-Feng Zhang, Zhi-Bo Wu, Ju-Ping Chen, Pu Li, and Wen-Dong Meng. The use of laser ranging to measure space debris. *Research in Astronomy and Astrophysics*, 12(2):212–218, 2012.

K. Riesing, H. Yoon, and K. Cahoy. A portable optical ground station for low-earth orbit satellite communications. In *2017 IEEE International Conference on Space Optical Systems and Applications (ICSOS)*, pages 108–114, 2017.

Toomas Erm, Zdenek Hurak, and Bertrand Bauvir. Time to go H_∞? In *Advanced Software, Control, and Communication Systems for Astronomy*, volume 5496, pages 68–79. International Society for Optics and Photonics, 2004.

Wodek Gawronski. Control and pointing challenges of large antennas and telescopes. *IEEE Transactions on Control Systems Technology*, 15(2):276–289, 2007.

Thomas Riel, Andras Galffy, Andreas Sinn, and Georg Schitter. Improvement of the angular precision of an optical metrology platform by disturbance compensation. In *Proceedings of the ASPE 2017 Spring Topical Meeting Precision Engineering and Optics, Tucson, Arizona, USA*, pages 15–20, 2017a.

Thomas Riel, Andras Galffy, and Georg Schitter. Analysis and robust control of an precision motion platform using disturbance compensation. In *Proceedings of the IEEE Conference on Control Technology and Applications (CCTA), Copenhagen, Denmark*, pages 1090–1095, 2018.

Kouhei Ohnishi, Masaaki Shibata, and Toshiyuki Murakami. Motion control for advanced mechatronics. *IEEE/ASME Transactions On Mechatronics*, 1(1): 56–67, 1996.

Pre-Print version of the article: Thomas Riel, Andras Galffy, Georg Janisch, Daniel Wertjanz, Andreas Sinn, Christian Schwaer, Georg Schitter, "High performance motion control for optical satellite tracking systems", *Advances in Space Research*, vol. 65, pp. 1333-1343, 2020. DOI: 10.1016/j.asr.2019.11.039

Wen-Hua Chen, Jun Yang, Lei Guo, and Shihua Li. Disturbance-observer-based control and related methods-an overview. *IEEE Transactions on Industrial Electronics*, 63(2):1083–1095, 2016.

Zamberi Jamaludin, Hendrik Van Brussel, and Jan Swevers. Friction compensation of an xy feed table using friction-model-based feedforward and an inverse-model-based disturbance observer. *IEEE Transactions on Industrial Electronics*, 56(10):3848–3853, 2009.

Jin Yang, Chuxiong Hu, Yu Zhu, Ze Wang, and Ming Zhang. Experimental investigation of shaping disturbance observer design for motion control of precision mechatronic stages with resonances. *Mechanical Systems and Signal Processing*, 92:334–348, 2017.

Thomas Riel, Rudolf Saathof, Andelko Katalenic, Shingo Ito, and Georg Schitter. Noise analysis and efficiency improvement of a pulse-width modulated permanent magnet synchronous motor by dynamic error budgeting. *Mechatronics*, 2017b.

Georg Kirchner, Daniel Kucharski, Franz Koidl, and Jörg Weingrill. Measuring atmospheric seeing with khz slr. In *Proceedings of International Laser Ranging Workshops, Canberra, Australia*, 2006.

Thomas Riel, Rudolf Saathof, Andelko Katalenic, and Georg Schitter. Tracking performance analysis and control of a small robotic telescope system. In *Proceedings of the 17th Advanced Maui Optical and Space Surveillance Technologies Conference, Maui, Hawaii, USA*, pages 1342–1349, 2016a.

Thomas Riel, Rudolf Saathof, Andelko Katalenic, and Georg Schitter. Noise analysis and improvement of a permanent magnet synchronous motor by dynamic error budgeting. In *Proceedings of the 7th IFAC Symposium on Mechatronic Systems, Loughborough University, UK*, pages 339–346, 2016b.

Lennart Ljung. *System identification: theory for the user*. Prentice-hall, 1987.

Rik Pintelon and Johan Schoukens. *System identification: a frequency domain approach*. John Wiley & Sons, 2012.

Karl J Åström and Björn Wittenmark. *Computer-controlled systems: theory and design*. Prentice-Hall, Inc., Upper Saddle River, New Jersey, 3 edition, 1997.

Carl J Kempf and Seiichi Kobayashi. Disturbance observer and feedforward design for a high-speed direct-drive positioning table. *IEEE Transactions on control systems Technology*, 7(5):513–526, 1999.

John C Doyle, Bruce A Francis, and Allen R Tannenbaum. *Feedback control theory*. Dover Publications, 2009.

Pre-Print version of the article: Thomas Riel, Andras Galffy, Georg Janisch, Daniel Wertjanz, Andreas Sinn, Christian Schwaer, Georg Schitter, "High performance motion control for optical satellite tracking systems", *Advances in Space Research*, vol. 65, pp. 1333-1343, 2020. DOI: 10.1016/j.asr.2019.11.039

Kemin Zhou, John Comstock Doyle, Keith Glover, et al. *Robust and optimal control*, volume 40. Prentice hall New Jersey, 1996.

Thomas S. Kelso. Celestrak. public domain satellite tracking data. https://www.celestrak.com/NORAD/elements/, 2018. Accessed: 27.09.2018.

M R Pearlman, John J Degnan, and JM Bosworth. The international laser ranging service. *Advances in Space Research*, 30(2):135–143, 2002.

Carey E. Noll. Crustal dynamics data information system. slr orbit predictions. ftp://cddis.gsfc.nasa.gov/slr/cpf_predicts/current/, 2018. Accessed: 27.09.2018.

Pre-Print version of the article: Thomas Riel, Andras Galffy, Georg Janisch, Daniel Wertjanz, Andreas Sinn, Christian Schwaer, Georg Schitter, "High performance motion control for optical satellite tracking systems", *Advances in Space Research*, vol. 65, pp. 1333-1343, 2020. DOI: 10.1016/j.asr.2019.11.039